Taylor & Francis
Taylor & Francis Group

Artificial Cells, Nanomedicine, and Biotechnology
An International Journal

ISSN: 2169-1401 (Print) 2169-141X (Online) Journal homepage: https://www.tandfonline.com/loi/ianb20

Antibacterial chitosan/silk sericin 3D porous scaffolds as a wound dressing material

Zeynep Karahaliloglu, Ebru Kilicay & Emir Baki Denkbas

To cite this article: Zeynep Karahaliloglu, Ebru Kilicay & Emir Baki Denkbas (2017) Antibacterial chitosan/silk sericin 3D porous scaffolds as a wound dressing material, Artificial Cells, Nanomedicine, and Biotechnology, 45:6, 1172-1185, DOI: 10.1080/21691401.2016.1203796

To link to this article: https://doi.org/10.1080/21691401.2016.1203796

ARTIFICIAL CELLS, NANOMEDICINE, AND BIOTECHNOLOGY, 2017
VOL. 45, NO. 6, 1172–1185
http://dx.doi.org/10.1080/21691401.2016.1203796

Taylor & Francis
Taylor & Francis Group

Antibacterial chitosan/silk sericin 3D porous scaffolds as a wound dressing material

Zeynep Karahaliloglu[a], Ebru Kilicay[b] and Emir Baki Denkbas[c]

[a]Aksaray University, Faculty of Science and Arts Biology Department, Aksaray, Turkey; [b]Zonguldak Vocational High School, Bülent Ecevit University, Turkey, Zonguldak; [c]Department of Chemistry, Biochemistry Division, Hacettepe University, Ankara, Turkey

ABSTRACT

Antimicrobial mixed dressings have traditionally been used to minimize bacterial infection of burns and other wounds. This study presents the advancement of biocompatible chitosan/silk sericin (CHT/SS) scaffolds combined with lauric acid (LA) and zinc oxide nanoparticles (nZnO) for the successful wound dressing applications. Antibacterial assay results showed that the diameters of the inhibition zone increased from 2 ± 0.4 to 7 ± 0.1 mm for *Escherichia coli*, as well as from 2.5 ± 0.2 to 6 ± 0.4 mm for *Staphylococcus aureus* while CHTS/SS/100nZnO compared to CHT/SS/0.01LA. The results not only showed excellent inhibition against Gram-positive and Gram-negative bacterial growth but also revealed improved proliferation and extended viability for HaCaT cells.

ARTICLE HISTORY
Received 11 May 2016
Revised 15 June 2016
Accepted 16 June 2016
Published online 8 July 2016

KEYWORDS
Chitosan; lauric acid; silk sericin; wound dressing; zinc oxide nanoparticles

Introduction

A wound is described as a fracture in the normal body integrity. Wound repair includes the activation of lots of intracellular and intercellular pathways for restoring tissue integrity and homeostasis (Gurtner et al. 2008). One of the most serious problems in wound repair is difficulty of the infection control in wound care. This is due to the injured part being the most unprotected to infection.

Wound dressings are very important for wound healing. The aim of wound healing is to heal the wound with minimal scarring and pain and preventing microbial invasion to the patient (Jannesari et al. 2011). Wound dressings protect the wound from contamination, side-infection, dryness, and bacterial invasion and they can be used for the treatment of severe skin burns and injuries through the delivery of bioactive agents to wound sites. The advanced dressings create and maintain a local moist environment around the wound to ease healing, absorb the wound fluids and exudates and minimize wound surface necrosis. The dressing materials must be also be biocompatible, biodegradable, elastic, and nonantigenic (Jakubiak et al. 2001). In addition, an ideal wound dressing should be a porous surface structure to ensure the gaseous exchange between the surface of the wound and the atmosphere.

Various wound healing dressings and devices are used in different physical forms such as skin scaffolds, gauzes, films, hydrogels, hydrocolloids, and xerogels (Boateng et al. 2008, Lloyd et al. 1998) and these different types of wound dressings rely on various materials that contain natural or synthetic polymers or their combinations. Some natural polymers that are present in the microporous structure improve wound healing by reason of its antimicrobial effectiveness. Chitosan (CHT), collagen, hyaluronic acid, and silicon can be currently used to make different wound dressings.(Moczar and Robert 1993, Turley and Torrance 1985). Among the natural polymers, CHT consists of glucosamine and N-acetyl glucosamine units linked by β (1–4) glycosidic bonds, and is a linear aminopolysaccharide. CHT, formed by N-deacetylation of chitin, is a polycationic polymer. It has an amazing physical and biochemical characteristics in wound healing applications as a dressing (Alves and Mano 2008, Berger et al. 2004, Florea et al. 2006) due to antibacterial, mucoadhesive, and hemostatic properties (Muzzarelli et al. 1999). Since CHT has amino groups and cationic in nature, it exhibits powerful activity against Gram-positive and Gram-negative bacteria and shows antibacterial activity versus to several pathogens like *Escherichia coli* or *Staphylococcus aureus* (Felt et al. 2000) at low concentrations. CHT induces type III collagen production in the wound environment and improves the proliferation and migration of fibroblasts, which promote the healing grade (Jiang et al. 2014). In addition, the nano and microparticles, combined with other materials such as powders, granules, and sponges, another form of CHT could be used to accelerate wound healing process (Shigemasa and Minami 1996).

On the other hand, silk, a natural protein, envelops sericin and fibroin. Silk sericin (SS) and their derivatives that have pharmacological properties are widely used to promote wound healing. SS, which surrounds the fibroin fiber, is a protein. It has a hydrophilic structure due to the presence of hydroxyl, amino, and carboxyl groups. It has promising features in the form of antioxidant, antibacterial, anticoagulant properties, excellent oxygen permeability, and a moisture organizing skill (Kurioka et al. 2004, Zhang 2002). There are many studies reported about sericin (Gimenes et al. 2007, Kim 2007), but, there are few studies with regard to the

CONTACT Emir Baki DENKBAŞ emirdenkbas@gmail.com Hacettepe University, Department of Chemistry, Beytepe/ANKARA/Turkey

preparation of antibacterial sericin scaffolds. Sericin can be mixed with other polymers in order to make scaffolds. Aramwit et al. fabricated sericin/PVA/glycerin scaffolds with good physical and biological properties through the use of the freeze drying technique. These scaffolds had a porous structure and were used as wound dressing application. When they were cultured with L929 mouse fibroblast cells, a lot of cells were found in the scaffolds prepared using the salt-leached method. (Aramwit et al. 2015).

In the event that there is a high infection risk into burns and other wounds, antimicrobial-impregnated dressings may be required. A wound dressing containing antimicrobial agent (e.g., silver, chlorhexidine, honey, and iodine) can be used to prevent the colonization of the wound and to improve the established infection. Silver (Ag), an effective antimicrobial agent, is most commonly used in burn wound management (Caruso et al. 2004). Dressings containing silver act by absorbing wound exudates, killing the microorganisms entering the dressing and sending silver onto the wound area. These active ions inhibit the replication, minimize growth, and metabolism via attaching to DNA, RNA, and proteins that are negatively charged. There have been several reviews regarding the use of silver dressings for wound management and the majority have concluded that there was not enough evidence to advise the use of dressings containing silver to prevent wound infection and promote wound healing (Storm-Versloot et al. 2010). Nevertheless, clinicians are still using silver dressings due to the absence of any alternatives and common marketing (Cutting et al. 2007). Besides, large amounts of silver have a toxic effect that it is hazardous to the wound (Poon and Burd 2004). For this reason, other antimicrobial-sucked dressings may have an important role to play in preventing the infection of wound. Among them, both zinc oxide nanoparticles and lauric acid (LA) have indicated powerful antimicrobial activity with less toxicity *in vitro*. LA, the strongest natural antimicrobial agent, a middle chain-free saturated fatty acid and a minor sebum component, indicates potent antimicrobial activity against many Gram-positive bacteria (Wille and Kydonieus 2003). It is also nontoxic and found in natural products. ZnO carries antibacterial, anti-inflammatory, and antifungal features and can be used in the manufacturing of sun protection cream, acne treatment and also wound dressings. Both wound's epithelialization effect and the bacteriostatic characteristic of ZnO improve the efficiency of it in wound dressings. ZnO nanoparticles have a broad spectrum of antibacterial capacity to improve wound healing (Kumar et al. 2012a, Singh et al. 2013).

In the present study, new CHT/SS scaffolds with high porosity as a wound dressing material were synthesized and characterized corresponding to physicochemical properties, biocompatibility and tested for antimicrobial activities. For this purpose, antibacterial agents, zinc oxide nanoparticles (nZnO) and LA incorporated into wound dressing materials in order to increase the antibacterial activity of them. In this study, we have indicated the powerful use of nZnO and LA, respectively, as alternative options for antibacterial therapy in wound healing application. Therefore, a CHT/SS dressing impregnated with nZnO and LA was tested against Gram-negative *E. coli* and Gram-positive *S. aureus*. The incorporation of different amounts of LA and nZnO into CHT/SS dressing material is a key factor to alter the scaffold characteristics. According to the inhibition test results, it was clearly seen that the LA-impregnated CHT/SS dressing was much more effective than the pure and nZnO-incorporated one. Consequently, both CHT/SS/nZnO and CHT/SS/LA with excellent antibacterial activity have promising scaffolds as a wound dressing composite materials.

Materials and methods

Materials

Bombxy mori (*B. mori*) silkworm cocoons were obtained from Kozabirlik (Bursa, Turkey). Low molecular weight CHT (with degree of deacetylation about 75–85%) with a number of average molecular weight of 22 kDa was purchased from Sigma-Aldrich (St. Louis, MO) as well as disodium carbonate (Na_2CO_3), LA and phosphate buffer saline (1× PBS). The commercial nZnO solution (an average particle size of ~35 nm) was obtained from Sigma–Aldrich (St. Louis, MO).

Immortalized human keratinocyte cell line (HaCaT) was obtained from Lonza (Basel, Switzerland). Cell culture grade chemicals include Dulbecco's modified Eagle's medium (DMEM, Sigma), L-glutamine, penicillin–streptomycin antibiotics, trypsin-EDTA and fetal bovine serum (Biological Industries, Kibbutz Beit-Haemek, Israel). MTT (4,5-Dimethylthiazol-2-yl)-2,5-Diphenyl tetrazolium bromide (MTT) and live/dead cell double-staining kit were obtained from Sigma-Aldrich (St. Louis, MO).

Isolation of SS protein from silk cocoons

Isolation of SS protein from *B. mori* cocoons was performed according to previously established protocols with slight modifications (Rockwood et al. 2011). In brief, *B. mo*ri silk cocoons were cut into small pieces and immersed in 0.05 M Na_2HCO_3 and autoclaved at 120 °C for 60 min. After extracting the structural fibroin protein from glue-like sericin protein through a filter paper, the sericin solution was cooled to a temperature of −80 °C (Revco ULT390–5-V31, Thermo Scientific, Asheville, NC) and the suspension was placed into a freeze-drying vessel (CHRIST ALPHA 2–4LD, Osterode, Germany) at a preset temperature of −70 °C for 24 h to remove the water phase completely.

Preparation of CHT/SS 3D scaffolds

Briefly, sericin powder was suspended in 2% (w/v) CHT solutions dissolved in 1% solution of acetic acid (v/v) at a 0.01:1 weight/volume ratio (w/v). After the homogenization procedure, antibacterial 3D porous CHT/SS scaffolds were prepared by the addition of nZnO and LA. For CHT/SS/nZnO scaffolds, 100 and 250 µl of the previously provided nZnO suspension were added dropwise to the abovementioned CHT/SS mixture. Similarly, LA was added to the mixture to prepare antibacterial CHT/SS/LA scaffolds with a weight ratio of 3.5/96/0.5% and 2.8/96/0.96%. CHT/SS/nZnO and CHT/SS/LA mixture kept vigorous stirring for 1 h to minimize the formation of agglomerates and sonicated to ensure nanoparticle dispersion. The

mixture was placed at a preset temperature of –70 °C for 24 h to remove the water phase completely and the samples were freeze-dried.

CHT/SS blends were made using epichlorohydrin (ECH) as a cross-linking agent. The prepared 3D porous scaffolds were cross-linked at a reaction temperature of about 70 °C under ECH vapor. The effect of the cross-linking reaction of the scaffolds was determined by Fourier transform infrared spectroscopy (Perkin Elmer SpectrumOne, Nicolet 520, USA). The spectra were recorded over the range of 500–4000 cm^{-1}.

Surface characterization of CHT/SS 3D scaffolds by scanning electron microscopy

The surface morphologies of freeze-dried antibacterial CHT/SS scaffolds were examined by scanning electron microscopy (SEM), using a JEOL JSM700F (JEOL, Welwyn Garden City, UK) at an operating voltage of 15 kV. For further examination, the antibacterial CHT/SS scaffolds were coated with gold/palladium in a sputter coater. In order to monitor the scaffolds seeded with cells for 2 days, the samples were fixed with paraformaldehyde solution (4%, w/v) for 2 h and then the samples were submerged in ethanol solutions (50, 70, 90, 100% v/v). Finally, the scaffolds were treated with hexamethyldisilazane (HMDS) for dehydration and coated with gold/palladium for SEM analysis.

Additionally, elemental composition analysis of CHT/SS scaffolds was conducted by coupled EDX with SEM.

Mechanical properties of CHT/SS 3D scaffolds

Compression testing was performed on the CHT/SS scaffolds (1.5 cm diameter; 1 cm height) using a universal testing-machine (Zwick, 250 kN, Ulm, Germany) at a constant compression rate of 10 mN/min. The tests were performed at room temperature. Compressive stress–strain curves were plotted and mechanical compression data were presented as an average of three tests.

Porosity of CHT/SS 3D scaffolds

The mean pore size and porosity percent of CHT/SS 3D scaffolds were determined by a mercury intrusion porosimeter (Quantachrome Corporation, Poremaster 60, Instruments, Boynton Beach, FL). The relationship between the applied pressure and the pore size i.e., the pore diameter distribution was determined according to the Washburn equation. Here, P is pressure, D is pore diameter, γ is the surface tension of mercury (480 dyne cm^{-1}) and θ is the contact angle between mercury and the pore wall, (commonly accepted at 140°).

$$D = (-4\gamma \cos\theta)/P$$

The measurements were obtained under low pressure and the pore size ranges from 200 to 4 μm.

In vitro release testing of nZnO from the CHT/SS 3D scaffolds

In order to study nZnO release from the 3D porous scaffolds, the nZnO-loading samples were incubated in phosphate-buffered saline solution (PBS, pH 7.4) at 37 °C for 10 days with continuous shaking. The buffer was collected (1 mL) at different incubation times and replenished using an equal volume of fresh PBS. At the end of the experiment, the samples were diluted 10 times with water. The amount of nZnO that had been released into the solution was measured by atomic absorption mass spectroscopy (AAS, ThermoFischer). This analysis was performed in triplicate for each time point with mean ± SD values reported.

In vitro cytotoxicity test and proliferation assay of CHT/SS 3D scaffolds

HaCaT were cultured in Dulbecco's Modified Eagle's Medium (DMEM), supplemented with 10% fetal bovine serum and 1% UI ml^{-1} penicillin–streptomycin and 1% L-glutamine in tissue culture flasks, at 37 °C, with 5% CO_2 in an incubator for maintenance. Cell culture studies were conducted on CHT/SS 3D porous scaffolds using MTT assay. MTT measures cell viability based on the activity of mitochondrial enzymes in live cells. So, the living cells reduced the MTT (3-[4,5-dimethylthiazol-2-yl]-2,5-diphenyltetrasodium bromide) substrate to a dark-blue formazan crystal and thus measured the mitochondrial activity of cells in a culture. Briefly, the samples were sterilized with 70% v/v ethyl alcohol for 30 min followed by washing three times in sterile PBS (pH 7.4) to remove alcohol. The 3D scaffolds were conditioned in the HaCaT-medium for 24 h (i.e., the extraction medium) and immortalized human keratinocytes were seeded onto each well of a 24-well plate at a density of 9×10^3 cells/well. After 24 h of cell seeding, the medium was changed to the extract of each scaffold and the cells were cultured for a further 24 h at 37 °C, with 5% CO_2 in an incubator. At the end of the exposure time, the cell culture medium was removed and 200 μl of MTT solution (5 μg/ml, diluted with RPMI 1640 without phenol red) was added to each well. Adding 200 μl of isopropanol/HCl mixture, the absorbance was read at 570 nm by a microplate reader (Biochrom Asys Expert Plus. Microplate Reader, Holliston, MA). Cell viability was calculated according to the following equation:

$$\text{Cell viability } (\%) = \frac{\text{A570(sample)}}{\text{A570(control)}} \times 100$$

where A570 is the absorbance value at 570 nm. The experiments were performed in triplicate, the results of which are presented as means.

Similarly, the cell proliferation on the CHT/SS 3D porous scaffolds was evaluated by the colorimetric assay. Briefly, the immortalized human keratinocyte cell line was maintained in DMEM supplemented with 10% FBS (Gibco, BRL, Gaithersburg, MD) and 1% penicillin–streptomycin and L-glutamine at 37 °C in a 5% CO2 incubator. The cells were harvested by trypsin/EDTA treatment. After sterilization of the 3D porous scaffolds using 70% v/v ethyl alcohol, the 3D porous scaffolds were incubated in 24-well tissue culture plates with HaCaT cells at a density of 9×10^3 cells/well for 1, 2, 3 and 4 days at 37 °C in 5% CO_2 incubator. The scaffolds were transferred to a new 24-well plate at the end of the predetermined time. Two hundred microliters of MTT reagent was pipetted as described

earlier into each well. After removal of the media at the end of 4 h, 200 μL of isopropanol/HCl mixture was added to the wells to dissolve the converted dye. The solution (100 μL) from each well was transferred to 96-well plates and the optical density (OD) was measured with a microplate reader (Biochrom Asys Expert Plus. Microplate Reader, Holliston, MA) at an absorbance of 570 nm.

Antibacterial studies

In vitro antibacterial activity of the prepared 3D porous scaffolds was qualitatively evaluated using the disc diffusion method. The antibacterial activities of pristine CHT/SS, CHT/SS/100nZnO, CHT/SS/250nZnO, CHT/SS/0.01LA, and CHT/SS/0.02LA were investigated against model microbial species including *E. coli* (Gram-negative) and *S. aureus* (Gram-positive). Microbial species *S. aureus* was grown in nutrient broth, whereas *E. coli* was grown in the Luria–Bertani medium overnight at 37 °C in a shaking incubator at a speed of at 250 rpm. Disc shape samples of 3D porous scaffold with $1.5 \times 1.5\ cm^2$ dimension were prepared and sterilized with UV-irradiation for 30 min. After the bacterial population was efficiently increased, the suspension of microbial species used for inoculation were prepared by adjusting fresh cultures at 0.5 Mac Farland standards (approximately 10^8 CFU/ml) and spectroscopically controlled. The inoculum was streaked on agar plates and air-dried under sterile conditions for 10 min. The samples in the form of small discs were placed carefully on *E. coli* and *S. aureus* culture plates and the agar plates were incubated at 37 °C for 24 h. The relative antibacterial activity was calculated by measuring the mean diameter of inhibition zones developed around the samples. All samples were studied in triplicate. Photographs of the inhibition zones were taken to support these obtained data and so, CHT/SS/nZnO and CHT/SS/LA were tested to check whether nZnO or LA present was actually responsible for Gram-positive and Gram-negative bacterial inhibition.

In vitro cell cytotoxicity

To visualize cell viability in the 3D porous scaffolds, the cells were stained using a live/dead cytotoxicity/viability kit included calcein-AM (live) and propidium iodide (dead) dye solutions. The assay is based on a cell-permeable dye for staining the live cells (calcein-AM) and a cell-impermeable dye for staining dead and dying cells (propidium iodide). For analysis, HaCaT cells (8×10^3 cells per well) were grown in DMEM supplemented with 10% fetal bovine serum and 1% penicillin–streptomycin at 37 °C, 5% CO_2. HaCaT cells were treated with pristine CHT/SS and composite 3D porous scaffolds which include different concentrations of nZnO and LA for 24 h period. The scaffolds and cell culture medium were subsequently removed and the cells were gently washed with PBS. They were then incubated in the mixture of calcein-AM and PI solution for 10 min at 37 °C (as per manufacturer's instructions). The cells were imaged using a fluorescence inverted microscope (Leica, Wetzlar, Germany) including Texas Red® and FITC filters. The tissue culture plate (TCP) was taken as a control for the double-staining test.

Statistical analysis

All quantitative experiments were performed in triplicate and results are expressed as mean values ± standard deviation (SD). Statistical analysis of data was performed by one-way analysis of variance (ANOVA). Results with p values of ≤ 0.05 and 0.005 were considered statistically significant.

Results and discussions

Characterization of CHT/SS 3D scaffolds by SEM

Four compositions of the CHT/SS (CHT/SS/100nZnO, CHT/SS/250nZnO, CHT/SS/0.01LA, and CHT/SS/0.02LA) were fabricated through freeze-drying techniques. Figure 1 depicts the SEM

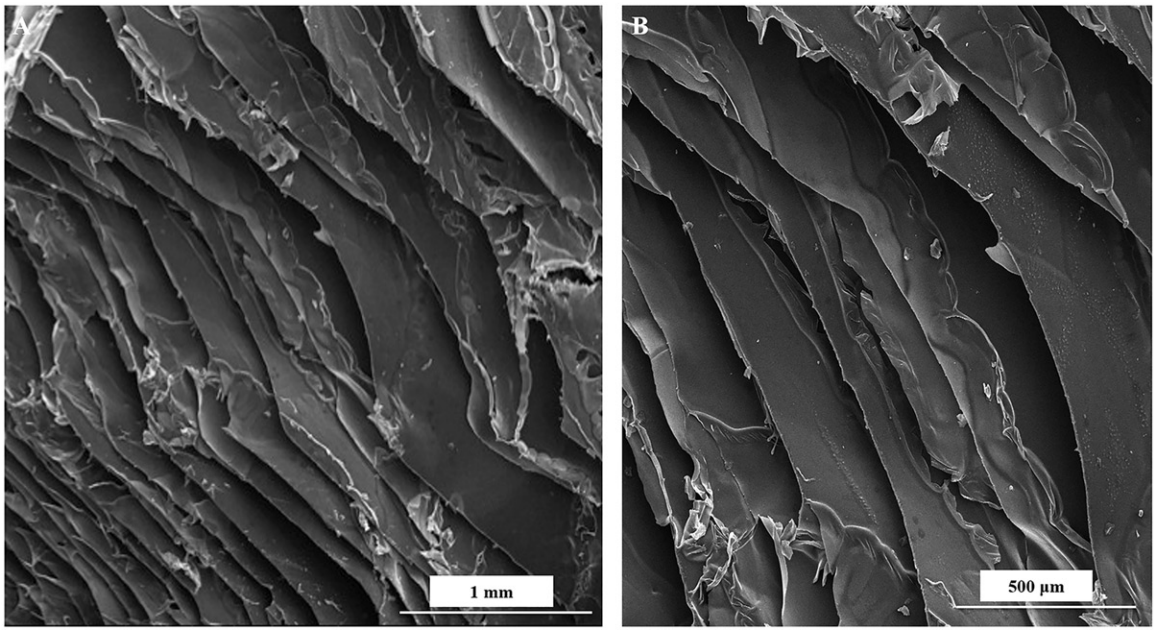

Figure 1. SEM images (A, B) of CHT/SS (1:0.01, w/v) composite 3D porous scaffolds.

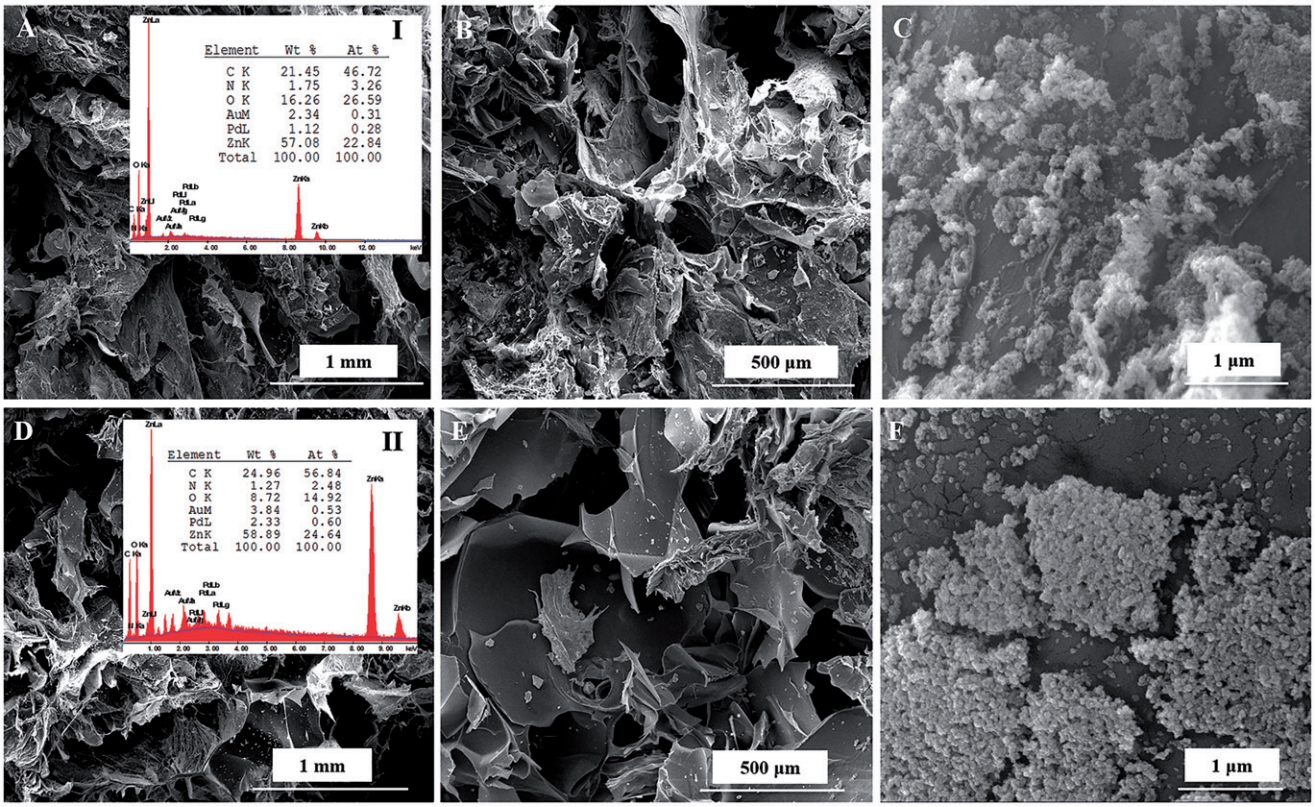

Figure 2. SEM images of CHT/SS/100nZnO (A–C) and CHT/SS/250nZnO (D–F) composite 3D porous scaffolds and EDX scan spectra of (I) CHT/SS/100nZnO, (II) CHT/SS/250nZnO.

images of the 3D porous scaffolds. Freeze-dried CHT/SS scaffolds show well-defined, porous structures with high pore interconnectivity.

In this work, we have prepared and characterized CHT/SS after incorporation of nZnO and LA. As previously reported, nZnO were in the size range approximately ~35 nm. Figures 2(A—F) shows the SEM images of the composite scaffolds reinforced with nZnO of two different concentrations. nZnO-reinforced CHT/SS scaffolds present a unique porous structure and the addition of ZnO NPs did not have any significant impact on the pore size or pore structure that could be observed in the SEM experiment. Figure 2(C) shows the representative images of surfaces recorded inside the pores of produced scaffolds. There is a clear presence of nZnO on the wall surface inside the pores and it probably has an influence on the bactericidal properties.

Figures 3(A—D) shows the SEM images of the LA-reinforced scaffolds. The representative images reveal that there were no LA residues on the wall surface of pores. It is important to note that biphasic scaffolds with good integration of two phases were developed. Most importantly, SEM images show homogenous distribution of pores which is a desirable feature for optimal cell distribution and cell proliferation in wound-dressing applications.

EDX and infrared analysis of CHT/SS 3D scaffolds

Figure 2(I—II) represents the EDX analysis of 3D porous antibacterial CHT/SS/nZnO scaffolds. EDX analysis results were used to confirm the presence of nZnO nanoparticles in the scaffolds of CHT/SS. Zn peak is the marker of choice for confirming the presence of nZnO nanoparticles in the scaffolds. The analysis of the data confirmed that nZnO nanoparticles were successfully incorporated into CHT/SS 3D porous scaffolds. Furthermore, it is significant that the increase in elemental peak of Zn corresponds to the predetermined concentrations of nZnO in composite scaffolds. The EDX spectra of the LA-reinforced scaffolds are illustrated in Figures 3(I—II). The presence of CHT and sericin in the 3D porous scaffolds was confirmed by the appearance of the characteristic peaks of oxygen, nitrogen, and carbon, which are the main components of CHT and sericin. Additional nitrogen peak increment was also observed in the EDX spectra of LA-reinforced 3D scaffolds. Furthermore, a new binding structure causes a decrease in the oxygen elemental value. These were attributed to the presence of LA in the structure.

Fourier transform infrared spectroscopy (FTIR) data of the pristine CHT/SS scaffolds have been compared with the LA and nZnO-reinforced scaffolds. SS had the characteristic peak of an amide I at 1656 cm^{-1}, an amide II at 1542 cm^{-1} and an amide III at 1246 cm^{-1} which were ascribed to the typical peaks of random coil structure (Figure 4(A)) (Srihanam et al. 2009). The peak positions are corresponded to C=O, N–H, and C–N stretching, C–N stretching and C=O bending, respectively. The peaks are characteristic of a random coil structure. The two bands at 1398 cm^{-1} and 1075 cm^{-1} were appointed to the C–H and O–H bending vibrations and the C–OH stretching vibration, respectively.

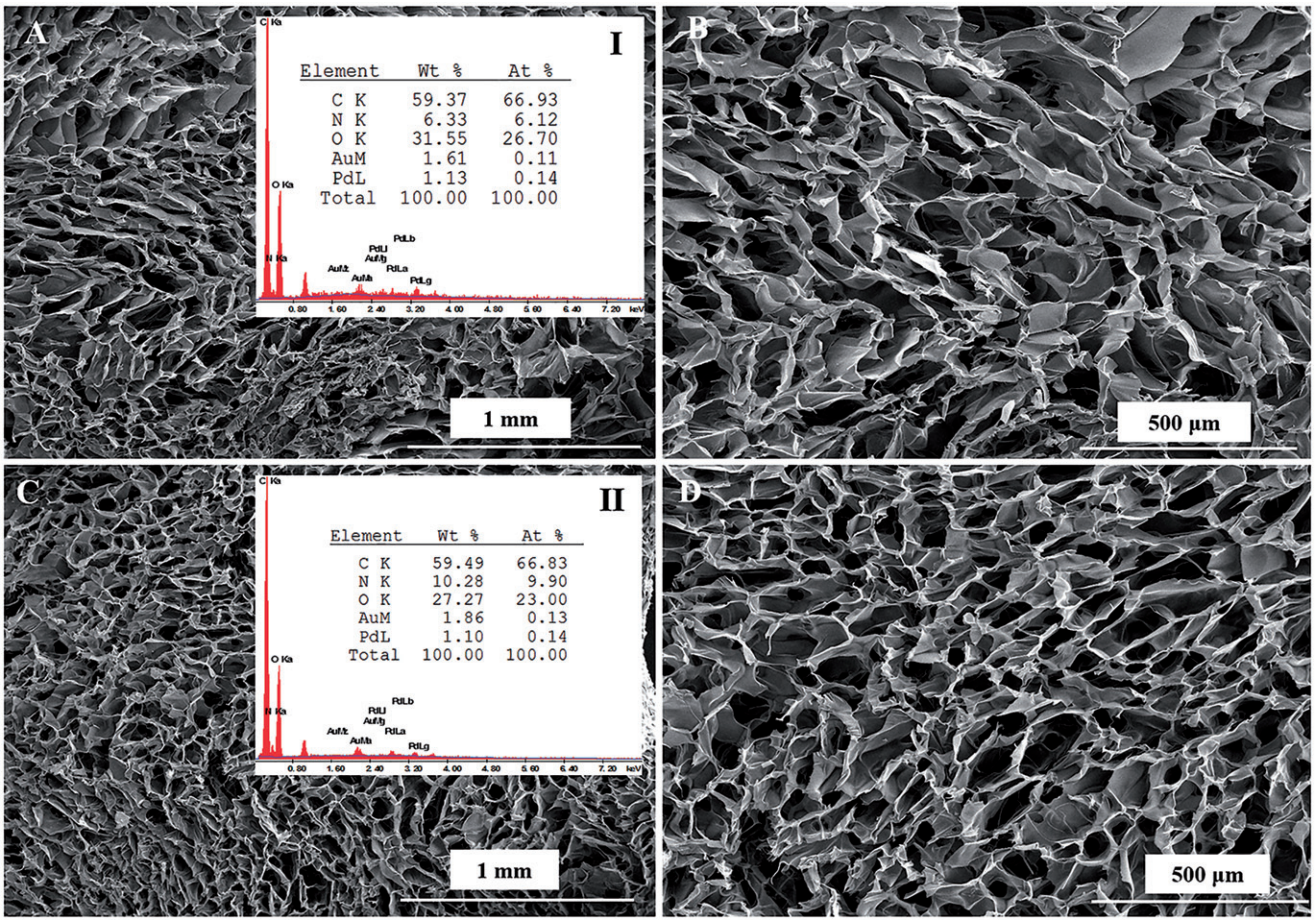

Figure 3. SEM images of CHT/SS/0.01LA (A, B) and CHT/SS/0.02LA (C, D) composite 3D porous scaffolds and EDX scan spectra of (I) CHT/SS/0.01LA and (II) CHT/SS/0.02LA.

These were due to the side-chain of abundant serine residues in the sericin (Srihanam et al. 2009). A typical FTIR spectrum of CHT shows a peak at 3303 cm^{-1} corresponding to $-NH_2$ and –OH groups' stretching vibration. The peaks at 2926 and 2856 cm^{-1} are attributed to asymmetric stretching of CH_3 and CH_2, whereas absorption band at 1627 cm^{-1} is determined as a bending vibration of $-NH_2$ group and stretching vibration of C=O group (Chen et al. 2015). As shown in Figure 4, the obtained characteristic peaks of the CHT and SS verify that they are well-integrated in the structure.

FTIR spectra of the nZnO-reinforced CHT/SS scaffolds in Figure 4(A) show a spread and intensification at 3446 cm^{-1} which are corresponding to the hydroxyl, amine, and amide groups of CHT (Li and Du 2003). The absorption band at 2866 cm^{-1} corresponding to the CH_2 asymmetric vibration shifted to 2846 cm^{-1}. A reduced intensity at 1450–1650 cm^{-1} that are attributed to the amide groups indicates the reinforcement of nZnO into the CHT/SS scaffolds (Tan and Arof 2006). Furthermore, the shifting in the sericin scan supported the interaction of the structure with nZnO. It can be seen in Figure 4(B) at the FTIR scans of LA-reinforced scaffolds, the peak located at 1711–1760 cm^{-1} assigned to C=O stretching of LA. The infrared spectrum obtained from CHT and sericin displayed all the characteristic peaks at the LA-reinforced scaffolds.

Mechanical properties of CHT/SS 3D scaffolds

A typical compressive stress/deformation curve of the pristine and LA and nZnO-reinforced 3D CHT/SS scaffolds are shown in Figure 5. The compressive strength of CHT/SS/0.02LA (205 kPa at 45% of deformation) was almost twice that of pristine CHT/SS ones (127 kPa at 45% of deformation) in the dry state. In contrast, the compressive strength of CHT/SS/nZnO and CHT/SS/0.01LA are similar to the pristine CHT/SS 3D scaffolds. The compressive strength values for CHTS/SS/250nZnO, CHTS/SS/100nZnO, and CHTS/SS/0.01LA are 159, 158, and 159 kPa at 45% of deformation, respectively. Jamuna-Thevi et al. reported the successful fabrication of a novel triple-layered poly(lactic-*co*-glycolic acid) (PLGA)-based composite membrane containing nanoapatite and LA. Tensile testing under dry conditions showed that the membranes containing 1 wt% and 2 wt% of LA exhibited a higher tensile strength and elastic modulus compared to pure PLGA membranes (Jamuna-Thevi et al. 2014). Furthermore, a composite from fly ash (FA) and recycled polypropylene (R) were developed using LA as a coupling agent. Nanoindentation tests results also demonstrated an increase in the mechanical properties in the case of the 1 and 2 wt % LA-coated composites in comparison to the uncoated counterpart (Sengupta et al. 2015).

The literature studies related to the effect of nZnO reinforcement on the mechanical properties of the scaffolds

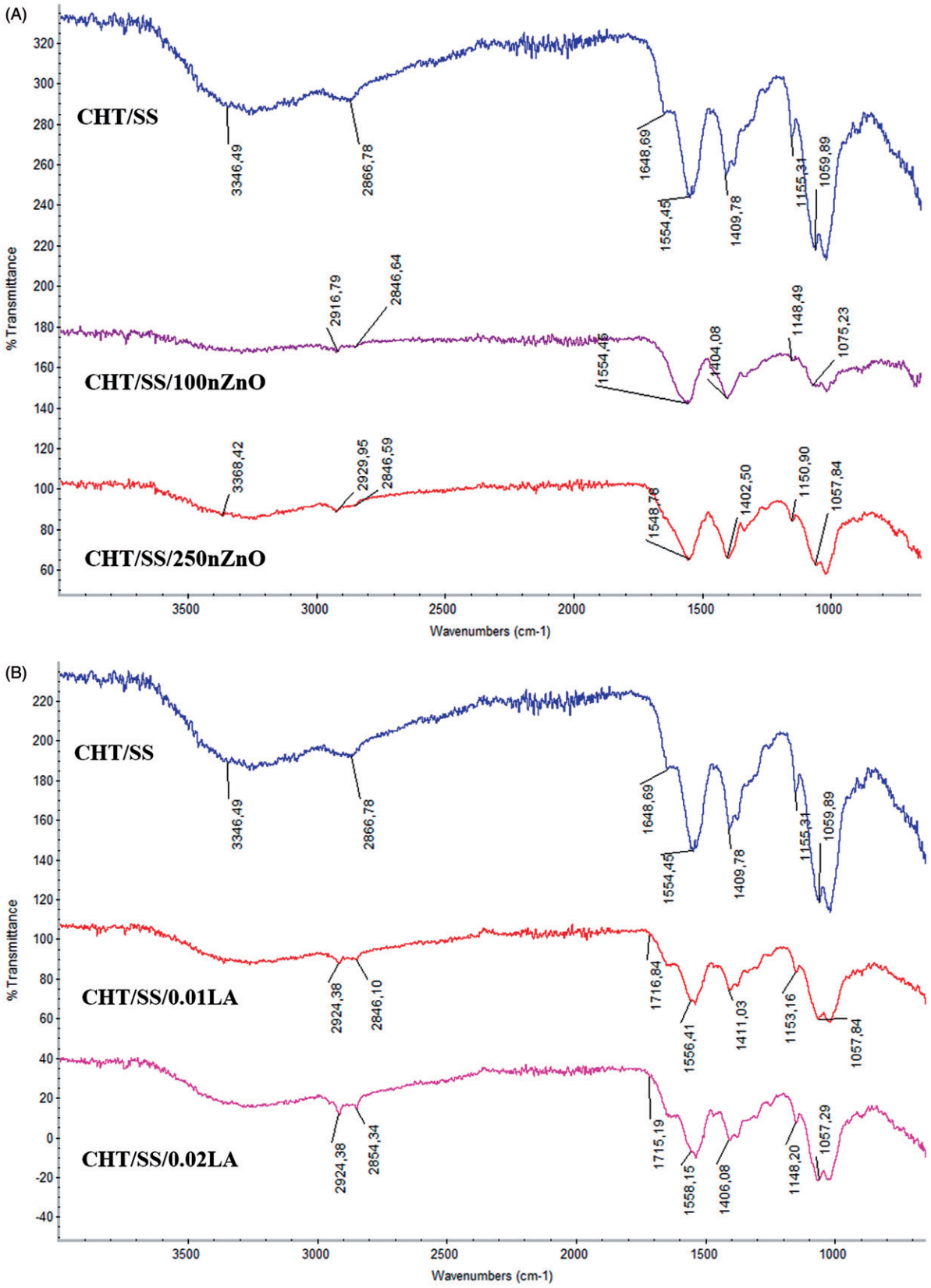

Figure 4. FTIR spectrum of CHT/SS, CHT/SS/100nZnO and CHT/SS/250nZnO (A) and CHT/SS/0.01LA and CHT/SS/0.02LA (B) 3D porous scaffolds.

produced indicate that nZnO has a significant effect on compression strength and fracture toughness (Shuai et al. 2016). Meshram et al. prepared novel CHT-gelatin/nZnO composites with enhanced antibacterial activity. After incorporating 1% nZnO into scaffolds, a significant increase in tensile strength of scaffolds was obtained (Meshram and Pawar 2015). Similarly, Hojati et al. indicated that the incorporation of nanoparticles into the resin composite resulted in an increase in

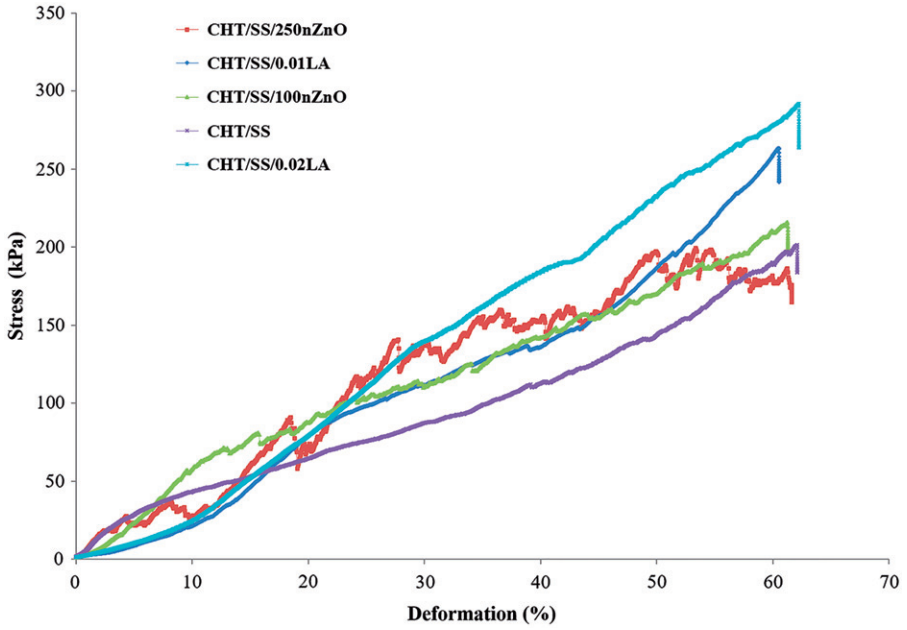

Figure 5. Stress-deformation curves of CHT/SS, CHT/SS/100nZnO, CHT/SS/250nZnO, CHT/SS/0.01LA and CHT/SS/0.02LA 3D porous scaffolds in dry-state.

the flexural modulus of the composites (Tavassoli et al. 2013). Inferior mechanical performances of the CHT/SS/nZnO 3D porous scaffolds compared to the LA-reinforced scaffolds in this study can be associated with the concentration of nZnO used.

Porosity of CHT/SS 3D scaffolds

The pore size distribution and % porosity of pristine and composite CTS/SS 3D porous scaffolds were tested using mercury intrusion porosimetry. The obtained % porosity values are shown in Figure 6. These % porosity values were approximately similar to each other. The results showed LA and nZnO-reinforced CHT/SS scaffolds having a porosity of 80% greater than that of pristine CHT/SS scaffolds. A high porosity and adequate pore size are essential factors in allowing high density cell seeding and maintaining efficient nutrient and oxygen supply to the seeded cells. It has been reported in the literature the optimum pore size and porosity in the range of 100–500 μm and 90%, respectively (Elsner et al. 2012, Ikada 2006).

Zhao et al. fabricated a dual-layer fiber dressing that included nitrofurazone (NFZ)-loaded poly(L-lactide) (PLLA)/sericin nanofibers as the first layer and NFZ-loaded PLLA nanofibers by electrospinning. The performance of these fiber-dressings as an ideal wound dressing were investigated and this research reported that different compositions of dual-layer fiber mats had porosities between 75.14 ± 5.43% and 78.35 ± 2.38% (Zhao et al. 2015). The obtained porosity percentage is high enough for usage as a wound-dressing material.

Using LA and nZnO, we obtained highly porous CHT/SS scaffolds with pore sizes in the range of 0–250 μm, indicating that pore size distribution of LA or nZnO-reinforced scaffolds well correspond to the pristine counterparts. The mean pore diameter was 25.32 ± 0.4 μm, 20.39 ± 0.3 μm, 21.51 ± 0.3 μm, 24.55 ± 0.4 μm and 24.05 ± 0.4 μm for CHT/SS, CHT/SS/100nZnO, CHT/SS/250nZnO, CHT/SS/0.01LA and CHT/SS/0.02LA, respectively. The data demonstrate that the doping of nZnO or LA to the structure does not change the pore size and distribution.

In vitro *release testing of nZnO from the CHT/SS 3D scaffolds*

A rapid antibacterial agent release is needed to clear the wound of contaminating microorganisms in infected wounds. *In vitro* release profile of CHT/SS/250nZnO and CHT/SS/100nZnO 3D porous scaffolds is displayed in Figure 7. A similar release pattern in both was obtained without the initial burst release in the first day. CHT/SS/100nZnO had the lower release in the fourth day compared to the first day while the relative concentration of Zn^{2+} after 5 days, measured for CHT/SS/250nZnO 3D porous scaffolds was much higher in comparison to the other content. The amount of Zn^{2+} ions released from the CHT/SS/250nZnO scaffold reached 0.25 mg/L after 10 days of incubation in PBS. Especially, CHT/SS/250nZnO 3D porous scaffolds showed prolonged release periods besides a slow and sustained release.

In vitro *cytotoxicity test and proliferation assay of CHT/SS 3D scaffolds*

The metabolic activity of cells, as determined by the MTT assay, is shown in Figure 8(A). The results indicate that there is no statistically significant difference between all samples. According to the classification criteria of toxicity reaction, a relative growth rate value higher than 75% is evaluated to be safe for the growth of cells (Chen et al. 2014). This graph shows over 75% cell viability on the CHT/SS scaffolds and it suggested that the fabricated pristine or composite scaffolds

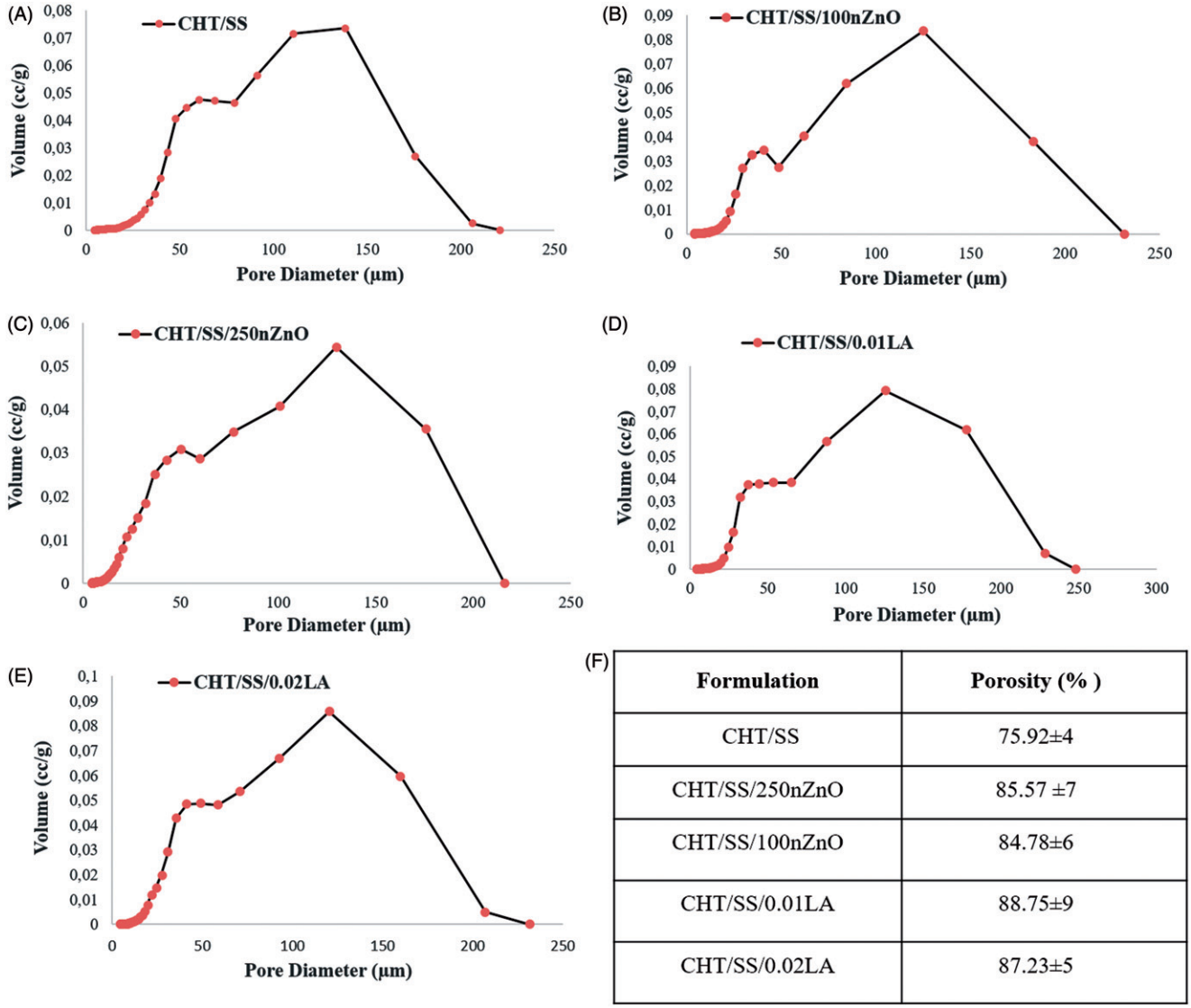

(F)

Formulation	Porosity (%)
CHT/SS	75.92±4
CHT/SS/250nZnO	85.57 ±7
CHT/SS/100nZnO	84.78±6
CHT/SS/0.01LA	88.75±9
CHT/SS/0.02LA	87.23±5

Figure 6. Pore histograms of (A) CHT/SS, (B) CHT/SS/100nZnO, (C) CHT/SS/250nZnO, (D) CHT/SS/0.01LA, (E) CHT/SS/0.02LA 3D porous scaffolds and (F) porosity percent of 3D porous scaffolds.

were noncytotoxic. MTT results confirmed that they had favorable properties for tissue engineering.

Figure 8(B) shows the results of the proliferation test carried out using MTT assay. Cell proliferation after culturing in day 1, 2, 3, and 4 of nZnO and LA-reinforced CHT/SS porous scaffolds were compared with the pristine CHT/SS porous scaffolds. At the end of the fourth day, the living cell concentration on the CHT/SS/100nZnO, CHT/SS/0.01LA, and CHT/SS/0.02LA is significantly higher than that of the pristine CHT/SS porous scaffold ($p < 0.005$). Similarly, we observed significant changes in cell proliferation between the CHT/SS/250nZnO and CHT/SS porous scaffolds at day 4 ($p < 0.05$). On the basis of the obtained absorbances on the third day, it was observed that LA- or nZnO-reinforcement improved the HaCaT cell adhesion and proliferation ($p < 0.05$). As shown in Figure 8, we tested the effect of different nZnO and LA concentrations on cell proliferation activity. The insignificant changes in cell proliferation were observed when the concentration of nZnO was increased to 250 µg. However, the LA-reinforced group did not exhibit toxic effect with various LA compositions. MTT data confirmed that LA induced an increase in the number of viable cells in a concentration-dependent manner compared to nZnO.

A published report has demonstrated that PLGA membranes modified with LA and hydroxy apatite is promising in terms of its cell compatibility resulting from good cell/membrane extracts interactions (Jamuna-Thevi et al. 2014). Furthermore, Augustine et al. investigated the effects of the PCL membrane containing different concentrations of nZnO on the proliferation and viability of adult goat fibroblast cells. They found that the PCL membranes containing 0.5 and 1% ZnO nanoparticles enhanced cell proliferation more compared to the neat PCL membrane (Augustine et al. 2014).

Cell adhesion behavior on the CHT/SS scaffolds with different contents of nZnO and LA was studied using HaCaT cells after incubation of two days and shown in Figure 9. The photographs indicated that the keratinocyte cells on scaffolds including nZnO and LA presented good cell adhesion and cytoplasmic extension and the adhered cells closely contacted with the scaffolds.

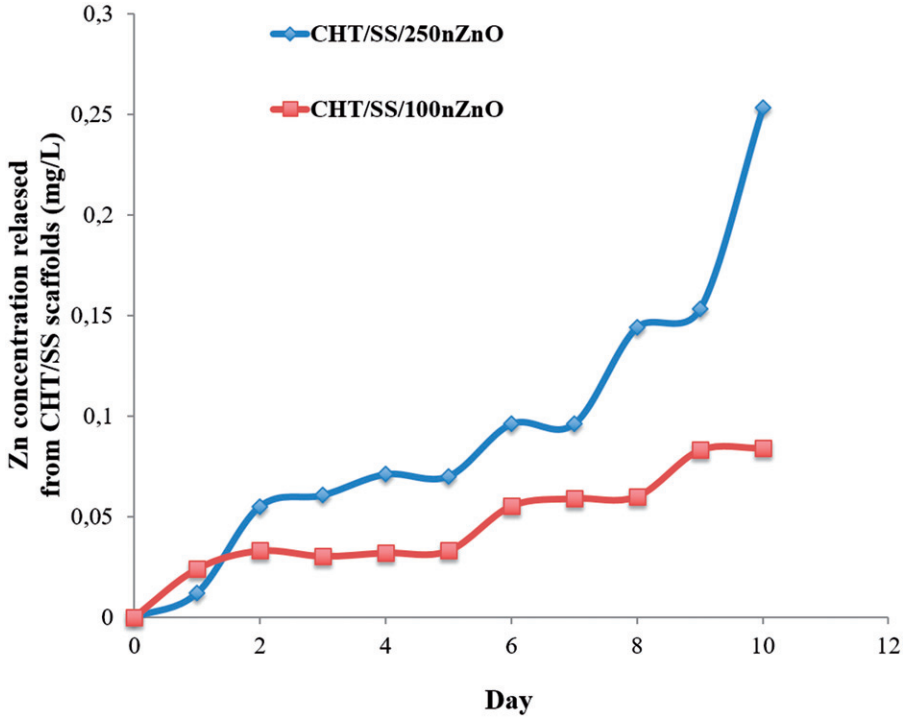

Figure 7. *In vitro* release profile of CHT/SS/250nZnO and CHT/SS/100nZnO 3D porous scaffolds.

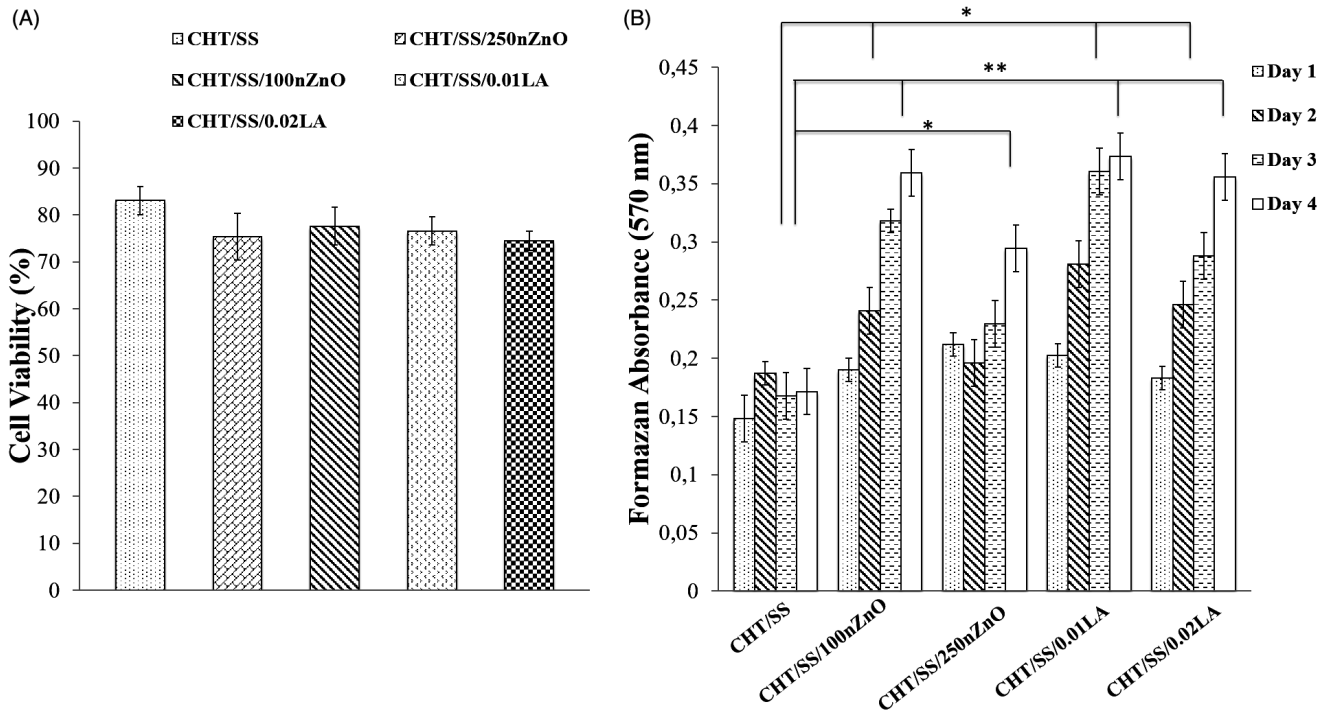

Figure 8. (A) *In vitro* cytotoxicity and (B) the cell proliferation of HaCaT cells on the pristine CHT/SS-, nZnO-, and LA-reinforced CHT/SS 3D porous scaffolds. Values are mean SEM; $n = 3$; $^{*}p < 0.005$, $^{**}p < 0.05$.

Live/dead assay

Additionally, in order to determine the cytotoxicity, HaCaT cells were incubated with porous scaffolds containing varying concentrations of nZnO and LA. The double-staining method was utilized to assess the viability in terms of cell death and the obtained photographs are given in Figure 10. The number of dead cells in all of the groups was clearly statistically nonsignificant in comparison to the number of live cells (Figure 10(A–E)). The results indicated that the insertion of nZnO and LA-content into the scaffolds had an optimum promotion effect for cell attachment and growth of HaCaT cells and presented nontoxicity to the cells.

Antibacterial activity

We had tested the antibacterial activity of pristine and nZnO/LA-reinforced CHTS/SS porous scaffolds against *S. aureus* and

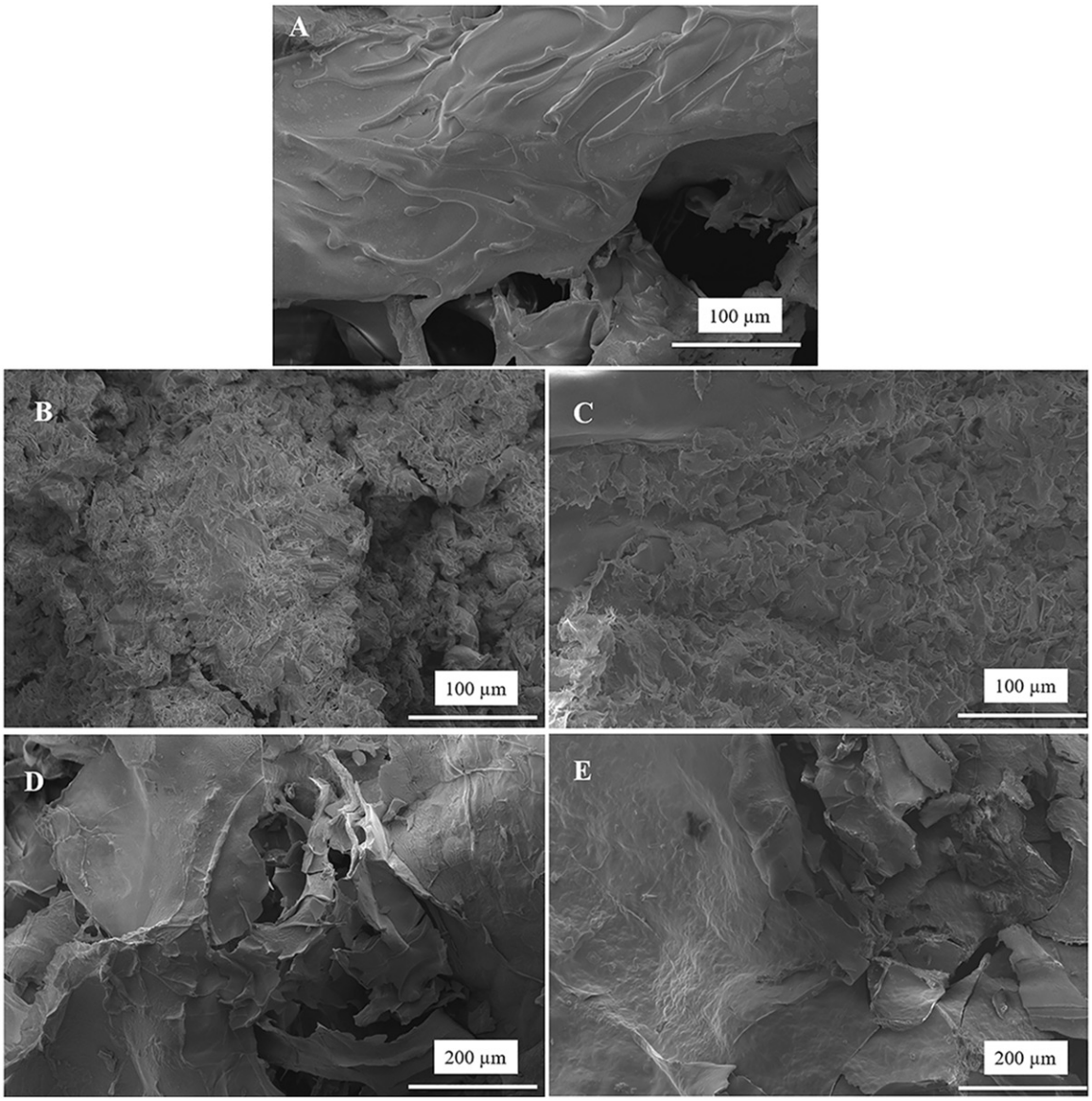

Figure 9. SEM images of the adhered HaCaT cells on the pristine (A) CHT/SS, (B) CHT/SS/0.01LA, (C) CHT/SS/0.02LA, (D) CHT/SS/100nZnO, and (E) CHT/SS/250nZnO. Scale bars are 100 and 200 µm.

E. coli (Table 1). Figure 11 shows the agar plates containing pristine and nZnO/LA-reinforced CHT/SS porous scaffolds. Pristine CHT/SS control did not show toxicity against the bacteria while the bacteria were inhibited to grow around both composite scaffold compositions. The data obtained revealed that CHT/SS scaffolds with higher concentration of nZnO and LA showed enhanced activity in comparison to the 3D porous scaffolds with lower concentrations of nZnO and LA. This could be attributed to the fact that nZnO or LA-reinforced scaffolds with higher concentrations are able to release significantly more zinc ions or LA than those with lower concentrations.

The antibacterial activity of nZnO and LA has been reported in the literature studies. nZnO produces reactive oxygen species (ROS) and the ROS or zinc ions attack the negatively charged bacterial cell wall and disintegrate the cell membrane (Prasanna and Vijayaraghavan 2015). LA is the most potent antimicrobial saturated fatty acid (Wille and Kydonieus 2003) and shows a strong antimicrobial activity against many Gram-positive bacteria that included *Staphylococcus* genus (Kitahara et al. 2004, Rouse et al. 2005).

Shalumon et al. prepared sodium alginate (SA)/poly (vinyl alcohol) (PVA) fibrous mats by electrospinning technique in their study. They reported that SA/PVA/ZnO mats showed an antibacterial activity due to the presence of ZnO against two different bacteria strains; *Staphylococcus aureus* and *E. coli* (Shalumon et al. 2011). Similary, Kumar et al. showed that chitin hydrogel/nZnO composite bandages enhanced the antibacterial activity through increasing the nZnO concentration (Kumar et al. 2012b). Furthermore, the literature review attested that LA has the greatest antibacterial activity (Chu-Kung et al. 2010, Ding et al. 2004).

Discussion

Here we report an alternative wound dressing material for obtaining an efficient wound healing process using nZnO and LA, which is a minor free fatty acid in sebum and has

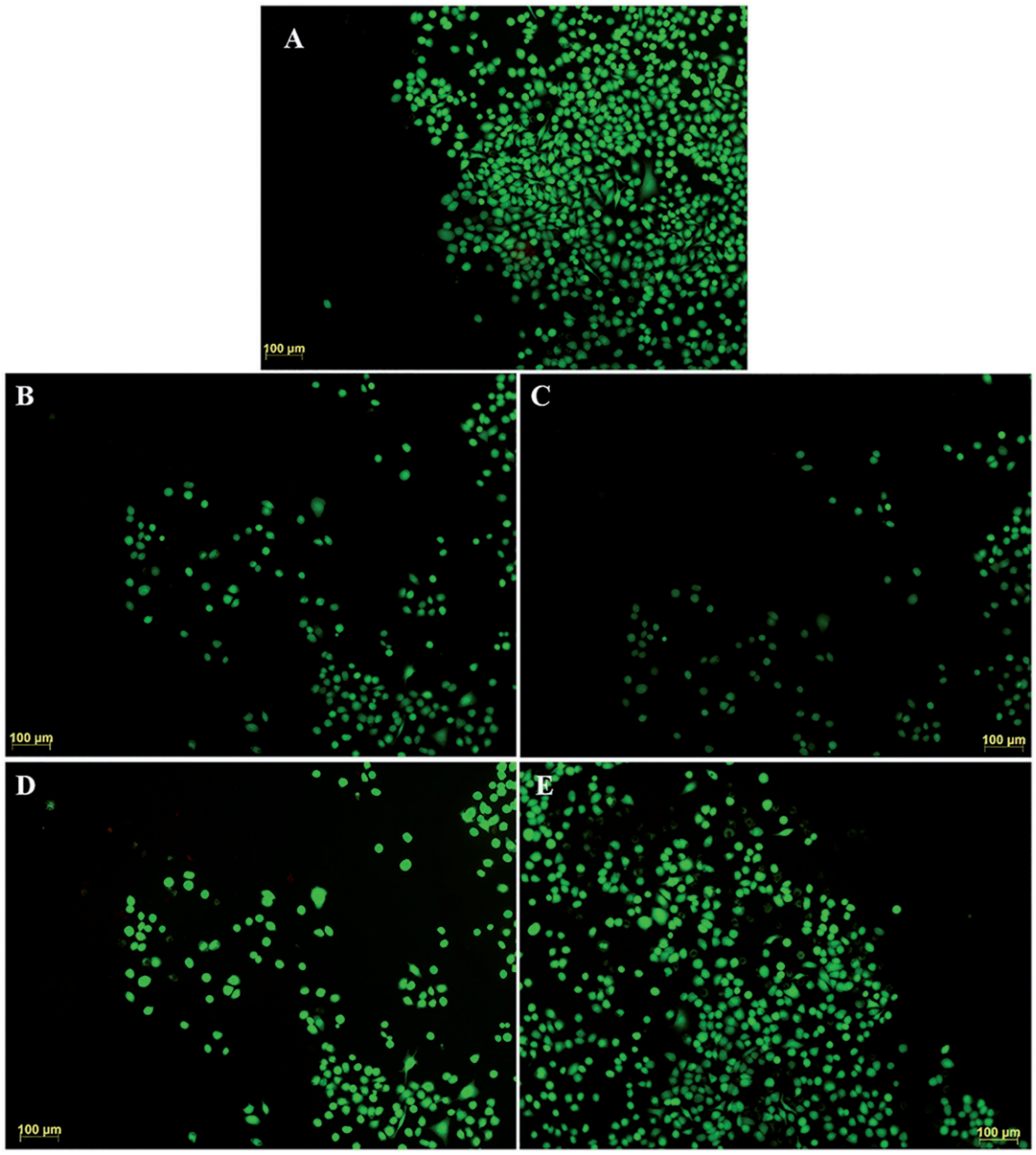

Figure 10. Fluorescence microscopy images of HaCaT cells after 24 h incubation with the extraction medium of 3D-porous scaffolds. (A) CHT/SS, (B) CHT/SS/250ZnO, (C) CHT/SS/250ZnO, (D) CHT/SS/0.01LA, and (E) CHT/SS/0.02LA. Scale bars are100 µm.

Table 1. Inhibition zone diameter of pristine and composite CHT/SS 3D porous scaffolds containing nZnO and LA in different concentrations.

	İnhibition zone diameter (mm)	
Formulation	*S. aureus*	*E. coli*
CHT/SS	0	0
CHT/SS/250nZnO	5.5 ± 0	4.5 ± 0
CHT/SS/100nZnO	2.5 ± 0.2	2 ± 0.4
CHT/SS/0.01LA	6.0 ± 0.4	7.0 ± 0.1
CHT/SS/0.02LA	8.0 ± 0.3	8.5 ± 0.2

antimicrobial activity. Interestingly, it is unknown whether LA reinforced into a 3D porous scaffold *in vitro* would have a similar effect; therefore, the potential of LA to be used as a wound dressing material is also unknown. In this study, we have demonstrated the potential of LA as an alternative option for antibacterial therapy in wound dressing application and the results were presented comparatively with nZnO.

In conclusion, 3D porous scaffolds were fabricated containing SS, CHT, nZnO and LA. FTIR studies and EDX confirmed the presence of the individual components. SEM images showed an interconnected microporous structure and the reinforcement of nZnO or LA had no influence on pore size and porosity. Moreover, positive antimicrobial effects were observed for CHT/SS/nZnO or CHT/SS/LA against two different bacterial strains; *E. coli and S. aureus*. However, CHT/SS/LA groups show a higher antimicrobial potential compared to the nZnO-reinforced groups. A double-staining assay showed that there was no damage of HaCaT cells in the presence of nZnO or LA. Most importantly, these nanocomposites 3D scaffolds improve the HaCaT cells' growth, attachment and proliferation and had no negative effect on the cytocompatibility of HaCaT cells. All the above results suggest that these 3D CHT/SS porous scaffolds have great potential to be used as wound dressing materials.

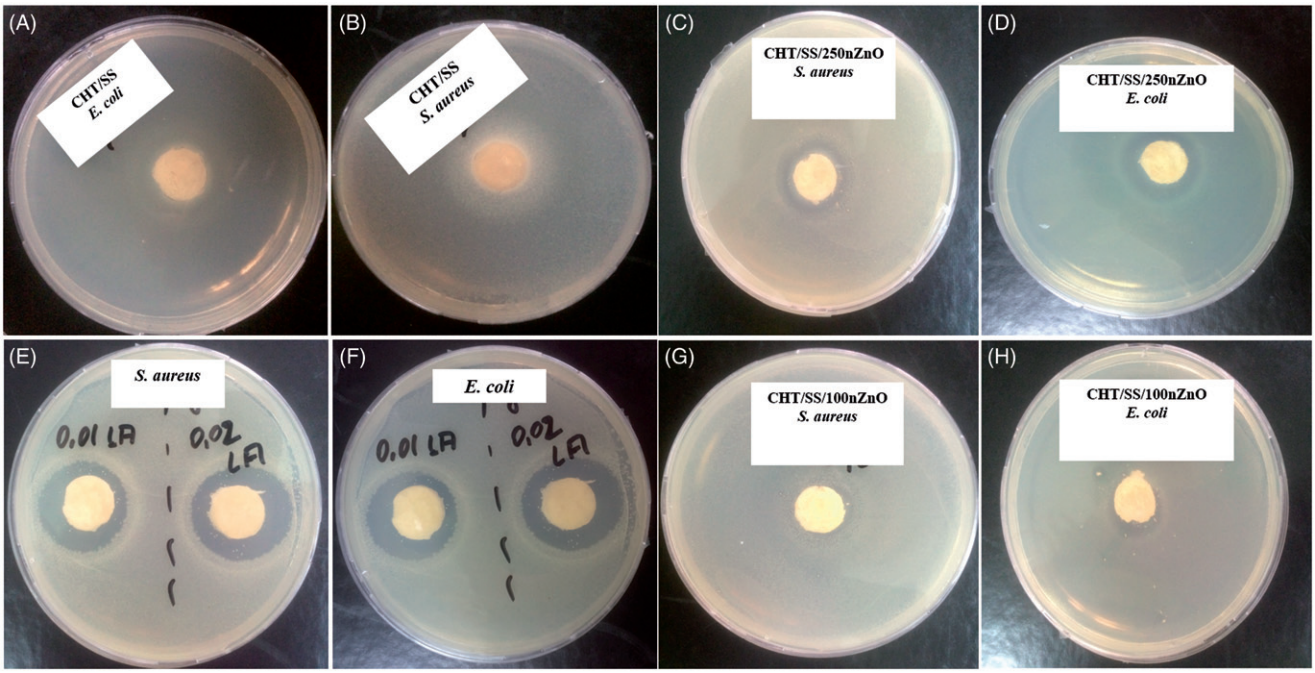

Figure 11. Antibacterial activity of pristine and composite CHT/SS 3D porous scaffolds containing nZnO and LA against *E. coli* and *S. aureus*.

Disclosure statement

The authors report no conflicts of interest. The authors alone are responsible for the content and writing of this article.

Funding information

This work was financially supported by the Bulent Ecevit University Research Fund (BEU-2015–33496813-01).

References

Alves NM, Mano JF. 2008. Chitosan derivatives obtained by chemical modifications for biomedical and environmental applications. Int J Biol Macromol. 43:401–414.

Aramwit P, Ratanavaraporn J, Ekgasit S, Tongsakul D, Bang N. 2015. A green salt-leaching technique to produce sericin/PVA/glycerin scaffolds with distinguished characteristics for wound-dressing applications. J Biomed Mater Res Part B. 103B:915–924.

Augustine R, Malik HN, Singhal DK, Mukherjee A, Malakar Kalarikkal N, Thomas S. 2014. Electrospun polycaprolactone/ZnO nanocomposite membranes as biomaterials with antibacterial and cell adhesion properties. J Polym Res. 21:347.

Berger J, Reist M, Mayer JM, Felt O, Peppas NA, Gurny R. 2004. Structure and interactions in covalently and ionically crosslinked chitosan hydrogels for biomedical applications. Eur J Pharm Biopharm. 57:19–34.

Boateng JS, Matthews KH, Stevens NE, Eccleston GM. 2008. Wound healing dressings and drug delivery systems: a review. J Pharm Sci. 97:2892–2923.

Caruso DM, Foster KN, Hermans MH, Rick C. 2004. Aquacel Ag in the management of partial thickness burns: results of a clinical trial. J Burn Care Rehabil. 25:89–97.

Chen H, Zhang E, Yang K. 2014. Microstructure, corrosion properties and bio-compatibility of calcium zinc phosphate coating on pure iron for biomedical application. Mater Sci Eng C. Mater Biol Appl 34:201–206.

Chen L, Hu J, Ran J, Shen X, Tong H. 2015. A novel nanocomposite for bone tissue engineering based on chitosan–silk sericin/hydroxyapatite: biomimetic synthesis and its cytocompatibility. RSC Adv. 5:56410–56422.

Chu-Kung AF, Nguyen R, Bozzelli KN, Tirrell M. 2010. Chain length dependence of antimicrobial peptide-fatty acid conjugate activity. J Colloid Interface Sci. 345:160–167.

Cutting K, White R, Edmonds M. 2007. The safety and efficacy of dressings with silver – addressing clinical concerns. Int Wound J. 4:177–184.

Ding B, Taotofa U, Orsak T, Chadwell M, Savage PB. 2004. Synthesis and characterization of peptide-cationic steroid antibiotic conjugates. Org Lett. 6:3433–3436.

Elsner JJ, Kraitzer A, Grinberg O, Zilberman M. 2012. Highly porous drug-eluting structures: from wound dressings to stents and scaffolds for tissue regeneration. Biomatter. 2:239–270.

Felt O, Carrel A, Baehni P, Buri P, Gurny R. 2000. Chitosan as tear substitute: a wetting agent endowed with antimicrobial efficacy. J Ocul Pharmacol Ther. 16:261–270.

Florea BI, Thanou M, Junginger HE, Borchard G. 2006. Enhancement of bronchial octreotide absorption by chitosan and N-trimethyl chitosan shows linear in vitro/in vivo correlation. J Control Release. 110:353–361.

Gimenes ML, Liu L, Feng X. 2007. Sericin/poly(vinyl alcohol) blend membranes for pervaporation separation of ethanol/water mixtures. J Membr Sci. 295:71–79.

Gurtner GC, Werner S, Barrandon Y, Longaker MT. 2008. Wound repair and regeneration. Nature. 453:314–321.

Ikada Y. 2006. Challenges in tissue engineering. J R Soc Interface. 3:589–601.

Jakubiak J, Sionkowska A, Linden LA, Rabek JF. 2001. Isothermal photo differential scanning calorimetry. Crosslinking polymerization of multifunctional monomers in presence of visible light photoinitiator. J Therm Anal Calorim. 65:435–443.

Jamuna-Thevi K, Saarani NN, Abdul Kadir MR, Hermawan H. 2014. Triple layered PLGA/nanoapatite/lauric acid graded composite membrane for periodontal guided bone regeneration. Mater Sci Eng C Mater Biol Appl. 43:253–263.

Jannesari M, Varshosaz J, Morshed M, Zamani M. 2011. Composite poly(vinyl alcohol)/poly(vinyl acetate) electrospun nanofibrous mats as a novel wound dressing matrix for controlled release of drugs. Int J Nanomed. 6:993–1003.

Jiang T, James R, Kumbar SG, Laurencin CT. 2014. Chitosan as a biomaterial: structure, properties, and applications in tissue engineering and drug delivery. In: Kumbar S., Laurencin C., Deng M. Eds. Natural and Synthetic Biomedical Polymers. Oxford: Elsevier, pp. 91–113.

Kim SJ. 2007. Gas Permeation Through Water-Swollen Sericin/PVA Membranes. ON, Canada: Waterloo.

Kitahara T, Koyama N, Matsuda J, Aoyama Y, Hirakata Y, Kamihira S, et al. 2004. Antimicrobial activity of saturated fatty acids and fatty amines against methicillin-resistant Staphylococcus aureus. Biol Pharm Bull. 27:1321–1326.

Kumar PT, Lakshmanan VK, Anilkumar TV, Ramya C, Reshmi P, Unnikrishnan AG, Nair SV, Jayakumar R. 2012a. Flexible and micro-porous chitosan hydrogel/nano ZnO composite bandages for wound dressing: in vitro and in vivo evaluation. ACS Appl Mater Interfaces. 4:2618–2629.

Kumar PT, Lakshmanan VK, Biswas R, Nair SV, Jayakumar R. 2012b. Synthesis and biological evaluation of chitin hydrogel/nano ZnO composite bandage as antibacterial wound dressing. J Biomed Nanotechnol. 8:891–900.

Kurioka A, Kurioka F, Yamazaki M. 2004. Characterization of sericin powder prepared from citric acid degraded sericin polypeptides of the silkworm, *Bombyx mori*. Biosci Biotechnol Biochem. 68:774–780.

Li Z, Du Y. 2003. Biomimic synthesis of CdS nanoparticles with enhanced luminescence. Mater Lett. 57:2480–2484.

Lloyd LL, Kennedy JF, Methacanon P, Paterson M, Knill CJ. 1998. Carbohydrate polymers as wound management aids. Carbohydr. Polym. 37:315–322.

Meshram JV, Pawar SH. 2015. Immobilization of zinc oxide nanoparticles in chitosan-gelatin composite membrane for antibacterial activity. Int J Pharm Bio Sci. 6:152–161.

Moczar M, Robert L. 1993. Stimulation of cell proliferation by hyaluronidase during in vitro aging of human skin fibroblasts. Exp Gerontol. 28:59–68.

Muzzarelli RA, Mattioli-Belmonte M, Pugnaloni A, Biagini G. 1999. Biochemistry, histology and clinical uses of chitins and chitosans in wound healing. Exs. 87:251–264.

Poon VKM, Burd A. 2004. In vitro cytotoxity of silver: implication for clinical wound care. Burns. 30:140–147.

Prasanna LV, Vijayaraghavan R. 2015. Insight into the mechanism of antibacterial activity of ZnO: surface defects mediated reactive oxygen species even in the dark. Langmuir. 31:9155–9162.

Rockwood DN, Preda RC, Yücel T, Wang X, Lovett ML, Kaplan DL. 2011. Materials fabrication from *Bombyx mor*i silk fibroin. Nat Protoc. 6:1612–1631.

Rouse MS, Rotger M, Piper KE, Steckelberg JM, Scholz M, Andrews J, Patel R. 2005. In vitro and in vivo evaluations of the activities of lauric acid monoester formulations against *Staphylococcus aureus*. Antimicrob Agents Chemother. 49:3187–3191.

Sengupta S, Ray D, Mukhopadhyay A, Sengupta S, Kar T. 2015. Lauric acid coated fly ash as a reinforcement in recycled polymer matrix composite. J Appl Poly Sci. 132:41586.

Shalumon KT, Anulekha KH, Nair SV, Nair SV, Chennazhi KP, Jayakumar R. 2011. Sodium alginate/poly(vinyl alcohol)/nano ZnO composite nanofibers for antibacterial wound dressings. Int J Biol Macromol. 49:247–254.

Shigemasa Y, Minami S. 1996. Applications of chitin and chitosan for biomaterials. Biotechnol. Genet. Eng. Rev.13:383–420.

Shuai C, Zhou J, Gao D, Gao C, Feng P, Peng S. 2016. Functionalization of Calcium Sulfate/Bioglass Scaffolds with Zinc Oxide Whisker. Moleules. 21:378.

Singh B, Sharma S, Dhiman A. 2013. Design of antibiotic containing hydrogel wound dressings: biomedical properties and histological study of wound healing. Int J Pharm. 457:82–91.

Srihanam P, Simcheur W, Srisuwan Y. 2009. Study on silk sericin and chitosan blend film: morphology and secondary structure characterizations. Pak J Biol Sci. 12:1487–1490.

Storm-Versloot MN, Vos CG, Ubbink DT, Vermeulen H. 2010. Topical silver for preventing wound infection. Cochrane Database Syst Rev. 3:CD006478.

Tan W, Arof AK. 2006. FT-IR studies on interactions among components in hexanoyl Chitosan-based polymer electrolytes, Spectrochim. Acta a: Mol Biomol Spectrosc. 63:677–684.

Tavassoli HS, Alaghemand H, Hamze F, Ahmadian BF, Rajab-Nia R, Rezvani MB, Kaviani M, Atai M. 2013. Antibacterial, physical and mechanical properties of flowable resin composites containing zinc oxide nanoparticles. Dent Mater. 29:495–505.

Turley EA, Torrance J. 1985. Localization of hyaluronate and hyaluronate-binding protein on motile and non-motile fibroblasts. Exp Cell Res. 161:17–28.

Wille JJ, Kydonieus A. 2003. Palmitoleic acid isomer (C16:1delta6) in human skin sebum is effective against gram-positive bacteria. Skin Pharmacol Appl Skin Physiol. 16:176–187.

Zhang YQ. 2002. Applications of natural silk protein sericin in biomaterials. Biotechnol Adv. 20:91–100.

Zhao R, Li X, Sun B, Tong Y, Jiang Z, Wang C. 2015. Nitrofurazone-loaded electrospun PLLA/sericin-based dual-layer fiber mats for wound dressing applications. RSC Adv. 5:16940–16949.